Letter

Non-Hermitian photonic spin Hall insulators

Rodrigo P. Câmara,[1] Tatiana G. Rappoport,[2,3] and Mário G. Silveirinha[1]

[1]*Instituto Superior Técnico and Instituto de Telecomunicações, University of Lisbon, Avenida Rovisco Pais 1, Lisboa, 1049001 Portugal*

[2]*Centro de Física das Universidade do Minho e do Porto (CFUMUP) e Departamento de Física, Universidade do Minho, P-4710-057 Braga, Portugal*

[3]*Instituto de Física, Universidade Federal do Rio de Janeiro, C.P. 68528, 21941-972 Rio de Janeiro, Rio de Janeiro, Brazil*

(Received 21 March 2023; revised 23 May 2024; accepted 28 May 2024; published 20 June 2024)

Photonic platforms invariant under parity ($\mathcal{P}$), time-reversal ($\mathcal{T}$), and duality ($\mathcal{D}$) can support topological phases analogous to those found in time-reversal invariant $\mathbb{Z}_2$ electronic systems with conserved spin. Here, we demonstrate the resilience of the underlying spin Chern phases against non-Hermitian effects, notably material dissipation. We identify that non-Hermitian, $\mathcal{PD}$-symmetric, and reciprocal photonic insulators fall into two topologically distinct classes. Our analysis focuses on the topology of a $\mathcal{PD}$-symmetric and reciprocal parallel-plate waveguide (PPW). We discover a critical loss level in the plates that marks a topological phase transition. The Hamiltonian of the $\mathcal{PTD}$-symmetric system is found to consist of an infinite direct sum of Kane-Mele-type Hamiltonians with a common band gap. This structure leads to the topological charge of the waveguide being an ill-defined sum of integers due to the particle-hole symmetry. Each component of this series corresponds to a spin-polarized edge state. Our findings present a unique instance of a topological photonic system that can host an infinite number of edge states in its band gap.

DOI: 10.1103/PhysRevB.109.L241406

Topological photonics [1,2] establishes a unique paradigm to create unidirectional channels immune to back-scattering. The topological protection of Chern insulators originates from an electromagnetic "quantum Hall effect" rooted in the time-reversal symmetry breaking [3,4]. Time-reversal invariant photonic structures also may host a plethora of topological phases [5–15], such as the optical counterpart of the quantum spin Hall state [16,17]. Due to the distinct nature of fermionic and bosonic systems, additional symmetries, such as duality symmetry which ensures balanced electric and magnetic responses, are essential for establishing $\mathbb{Z}_2$ topological protection in photonic platforms [9,18].

To our best knowledge, the most general symmetry transformation that can enable the $\mathbb{Z}_2$ topological protection in photonic systems is a combination of the parity ($\mathcal{P}$), time-reversal ($\mathcal{T}$), and duality ($\mathcal{D}$) operators, $\tilde{\mathcal{T}} = \mathcal{PTD}$ [9,18–20]. The $\tilde{\mathcal{T}}$ operator may be regarded as a pseudo-time-reversal operator, as it is antilinear and satisfies $\tilde{\mathcal{T}}^2 = -\mathbf{1}$. This property ensures that photonic states in a $\mathcal{PTD}$ symmetric system are degenerate, in accordance with Kramers' theorem [9,18]. Moreover, it implies the existence of a basis where the system's scattering matrix is anti-symmetric [18]. Importantly, in systems with an odd number of bidirectional propagation channels, this property implies that light transport can occur without back-reflections [18].

Recently, the study of topological phases was extended to non-Hermitian systems through a generalization of the notion of band gaps to complex spectra [21–33]. However, previous studies on $\mathcal{PTD}$-symmetric systems dealt exclusively with energy conserving (Hermitian) platforms [19,20,34–36]. Here, we study the impact of non-Hermitian effects, notably material dissipation, on the topological phases of $\mathcal{PTD}$-symmetric systems. In time-reversal-invariant electronic systems, the topological protection of the edge channels is stronger when spin is also conserved [37]. A mapping can be established between the $\mathbb{Z}_2$ invariant and the $\mathbb{Z}$-valued Chern numbers associated with the spin sectors [38]. The topological indices of the spin sectors offer the most comprehensive description of the properties of the edge states. In $\mathcal{PTD}$-invariant optical platforms, light modes also have a preserved polarization (pseudospin). Therefore, we focus on the $\mathbb{Z}$-valued Chern numbers of the pseudospin sectors. We discover that these topological indices demonstrate remarkable resilience to material absorption. Notably, we identify a topological phase transition controlled by the strength of the loss parameter. This transition is characterized by exceptional mode degeneracies and resonant energy absorption. Moreover, the topological charge of our system is characterized by a nonconvergent sum of integers. This distinct feature is a consequence of the particle-hole symmetry of the spectrum of photonic systems and is manifested by the emergence of an infinite number of edge states within the topological band gap.

Our system consists of a parallel-plate waveguide [see Fig. 1(a)], where the electromagnetic responses of the top and bottom plates are interconnected through electromagnetic duality [19,39]. Each plate is modeled by an impedance boundary condition, defined as $Z_i\,\hat{\boldsymbol{n}} \times \boldsymbol{H} = \boldsymbol{E}_{\rm tan}$ with $\hat{\boldsymbol{n}}$ the unit normal vector to the plate, oriented towards the dielectric. Here, $\boldsymbol{E}_{\rm tan}$ is the tangential electric field and Z_i the surface impedance of the $i = +/-$ (top/bottom, respectively) plate. Similar to Ref. [18], we consider the parity transformation $(x, y, z) \to (x, y, -z)$ that exchanges the positions of the plates, and the duality mapping $\mathcal{D} : (\boldsymbol{E}, \boldsymbol{H}) \to (\boldsymbol{H}Z_0, -\boldsymbol{E}/Z_0)$ that converts $Z_+ \to Z_-$ and vice versa (Z_0 is the vacuum impedance). The composition of these two transformations leaves the air region of the guide unaltered. The system is

 ©2024 American Physical Society

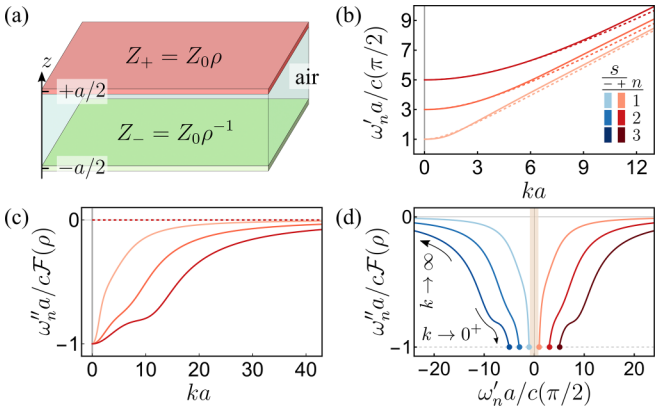

FIG. 1. (a) Structure of the $\mathcal{PD}$-symmetric parallel-plate waveguide with a dielectric block (air) of width a in between two impedance surfaces. (b) Real ω_n' and (c) imaginary ω_n'' parts of the eigenfrequencies as functions of k. We choose $s = +$ (positive bands) and consider the first few guided modes: $n = 1, 2, 3$. Dashed (solid) curves refer to $\rho = 0$ ($\rho = 0.6$). ω_n'' in (c) is normalized to the function $\mathcal{F}(\rho)$. (d) Projected band structure in the complex plane for the case $\rho = 0.6$. Positive (negative) frequency branches are in red (blue). The frequency values for $k = 0$ are marked by solid dots.

parity-duality ($\mathcal{PD}$) symmetric if and only if the two surface impedances satisfy $Z_+Z_- = Z_0^2$ [40].

For simplicity, we assume the surface impedances $Z_\pm$ to be real and frequency independent, defined as $Z_\pm = Z_0\rho^{\pm 1}$, where ρ is the normalized resistivity parameter. When $\rho = 0$, the plates act as perfect electric (PEC) or magnetic (PMC) conductors, as in Ref. [19]. In our analysis, ρ is allowed to span real values. Positive ρ values indicate that the plates are dissipative. Conversely, negative ρ values correspond to active (amplifying) plates. The waveguide is Hermitian and time-reversal invariant ($\mathcal{PT}\mathcal{D}$-symmetric) only when $\rho = 0$.

In the following, we denote a point in space (x, y, z) by (z), and the mirror-symmetric point $(x, y, -z)$ by $(-z)$. For $\mathcal{PD}$-symmetric and *reciprocal* systems, such that $\varepsilon(z) = \mu(-z)$, the frequency-domain (source-free) Maxwell equations can be split into two independent sets of equations [19]

$$\pm\frac{ic}{\varepsilon(z)}\begin{pmatrix} 0 & \partial_z & \partial_y \\ -\partial_z & 0 & -\partial_x \\ \partial_y & -\partial_x & 0 \end{pmatrix}\boldsymbol{\Psi}^\pm(-z) = \omega\boldsymbol{\Psi}^\pm(z), \quad (1)$$

that are formally equivalent to $\hat{\mathcal{H}}^\pm\boldsymbol{\Psi}^\pm(z) \equiv \omega\boldsymbol{\Psi}^\pm(z)$ with the eigenstates $\boldsymbol{\Psi}^\pm$ written in terms of the electric and magnetic fields $\boldsymbol{E}$ and $\boldsymbol{H}$ as $\boldsymbol{\Psi}^\pm(z) = [E_x(z) \mp Z_0H_x(-z), E_y(z) \mp Z_0H_y(-z), E_z(z) \pm Z_0H_z(-z)]^\intercal$ [19]. The "polarization" associated with the superscript "+" or "−" is conserved and represents an internal degree of freedom. We refer to it as pseudospin and to the modes $\boldsymbol{\Psi}^\pm$ as pseudospinors, following the terminology of topological photonics. Here, c denotes the speed of light in vacuum and ω is the oscillation frequency. As $\boldsymbol{E} = \frac{1}{2}(\boldsymbol{\Psi}^+ + \boldsymbol{\Psi}^-)$, the dynamics of the electric field is controlled by the dynamics of the two pseudospinors [Eq. (1)]. Different from the original Maxwell's equations, the dynamics of the pseudospinors is strongly nonlocal, as the two sides of Eq. (1) are evaluated at mirror-symmetric points. Interestingly, the pseudospin decomposition remains valid even when the plate walls or the dielectric are lossy. In our guide, the dielectric is air ($\varepsilon = \mu = 1$), so that non-Hermitian effects arise exclusively due to the plates.

In the Hermitian case, where both the dielectric and the plates are lossless, the eigenstates with pseudospin "+" can be transformed into eigenstates with pseudospin "−" using the time-reversal operator. While such a construction is not feasible in the non-Hermitian case, a crucial observation is that the electromagnetic reciprocity of the system guarantees that the total topological charge vanishes [21], similar to the fermionic case [44]. Thereby the Chern indices of the operators $\hat{\mathcal{H}}^\pm$ in Eq. (1) must be exactly balanced: $\mathcal{C}^+ + \mathcal{C}^- = 0$. Therefore, $\mathcal{PD}$-symmetric reciprocal systems may host nontrivial topological phases determined by the invariant $\mathcal{C}^+ = -\mathcal{C}^-$. In the following, we apply the non-Hermitian topological band theory to determine the phase diagram of the nonlocal operators $\hat{\mathcal{H}}^\pm$ [22].

Since the system is invariant under continuous translations in the xoy plane, the eigenstates can be factorized as $\boldsymbol{\Psi}^\pm(\boldsymbol{r}, t) = \boldsymbol{\Psi}^\pm_{\boldsymbol{k}}(z)e^{-i\omega t}e^{i\boldsymbol{k}\cdot\boldsymbol{r}}$, where $\boldsymbol{k}$ is an in-plane real-valued wave vector of magnitude k. The pseudospinors are found by first solving Maxwell's equations subject to the appropriate boundary conditions in the guide, and then projecting the field solutions onto the pseudospinor subspaces [40]. Because the PPW is also invariant under arbitrary rotations around the z-axis, it is convenient to write the eigenstate in terms of the unit vectors $(\hat{\boldsymbol{k}}, \hat{\boldsymbol{z}} \times \hat{\boldsymbol{k}}, \hat{\boldsymbol{z}})$. In this basis, the coordinates of the pseudospinors are

$$\boldsymbol{\Psi}^\pm_{\boldsymbol{k},n}(z) \propto \begin{pmatrix} \mp(e^{-i\kappa_n z} + h_n e^{i\kappa_n z}) \\ -\frac{\omega_n}{c\kappa_n}(e^{i\kappa_n z} - h_n e^{-i\kappa_n z}) \\ \mp\frac{k}{\kappa_n}(e^{-i\kappa_n z} - h_n e^{i\kappa_n z}) \end{pmatrix}, \quad (2)$$

where $n = 1, 2, \ldots,$ labels different modes, κ_n is a transverse wave number, ω_n is the eigenfrequency, and $h_n \equiv e^{i\kappa_n a}\frac{\omega_n - c\rho\kappa_n}{\omega_n + c\rho\kappa_n}$. For each k real-valued, the transverse wave number satisfies the modal equation

$$e^{2i\kappa_n a} = \frac{\omega_n + c\rho\kappa_n}{\omega_n - c\rho\kappa_n}\frac{\rho\omega_n + c\kappa_n}{\rho\omega_n - c\kappa_n}, \quad (3)$$

with $\omega_n = s \times c\sqrt{k^2 + \kappa_n^2}$ and $s = \pm$. Each eigenmode is associated with an in-plane wave vector $\boldsymbol{k}$, with an integer n that identifies the band and with $s = \pm$ that specifies the square root branch. Importantly, the modal equation is independent of the pseudospin, resulting in an identical spectrum for the operators $\hat{\mathcal{H}}^\pm$. When $k = 0$, the modal equation yields analytical solutions $\kappa_n = (2n - 1)\pi/2a - s \times i\mathcal{F}(\rho)/a$ [40] with $\mathcal{F}(\rho) = \mathrm{sgn}(\rho)\ln\left|\frac{|\rho|+1}{|\rho|-1}\right|$. These solutions are extended numerically to $k > 0$ via a Nelder Mead minimization scheme [40], allowing us to obtain the corresponding frequencies. We shall see that the singularities $\rho = \pm 1$ in the function $\mathcal{F}(\rho)$ play an important role in the topological properties of the waveguide.

Figures 1(b) and 1(c) show how the real ω_n' and imaginary ω_n'' frequency parts vary with k, in systems with $\rho = 0$ (dashed lines) and $\rho = 0.6$ (solid lines). If the system is conservative ($\rho = 0$), the modal Eq. (3) reduces to $e^{2i\kappa_n a} = -1$, so the frequencies are real-valued, as expected. In the dissipative case ($\rho = 0.6$), the frequencies exhibit complex values.

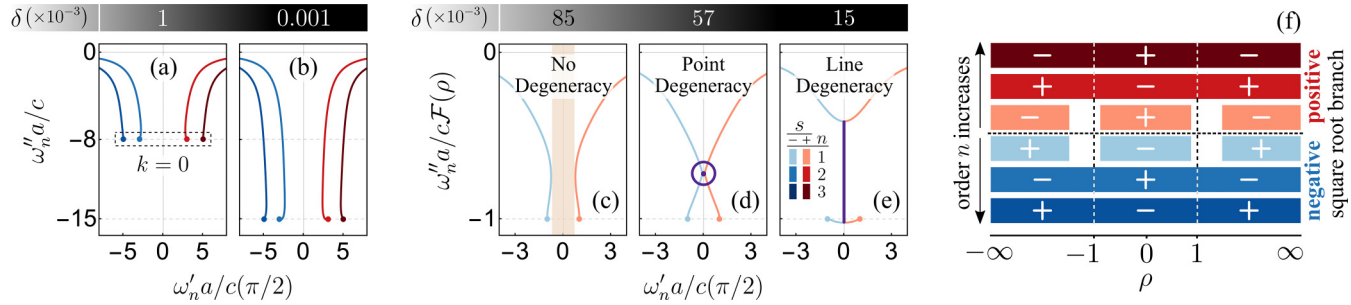

FIG. 2. (a), (b) High-order ($n = 2, 3$) frequency bands projected on the complex plane, with (a) $\delta = 1 - |\rho| = 10^{-3}$ and (b) $\delta = 10^{-6}$. The frequencies associated with $k = 0$ are represented by solid dots. (c)–(e) First-order branches ($n = 1$) near the critical resistivity $\rho = 1$ ($\delta \to 0^+$). (f) Topological phase diagram. The values of $\mathcal{C}_n^+$ are given for the range of ρ where they are defined. The gap is closed in the white-shaded regions, near $\rho = \pm 1$.

Figure 1(d) displays the projected band structure for $\rho = 0.6$, representing the locus of $\omega_n(k)$ for all k real-valued. Notably, the diagram exhibits a mirror symmetry about the imaginary frequency axis: $\omega_n \to -\omega_n^*$. This symmetry, stemming from the reality of the electromagnetic field, correlates the positive and negative parts of the photonic spectrum ($s = \pm$), and is known as the particle-hole symmetry [40]. The positive and negative frequencies are separated by a gap on the complex plane (beige vertical strip). The frequency branches are disjoint, meaning they exhibit no intersections or self-intersections. These characteristics are typical of the band structure, except when the resistivity approaches $\rho = \pm 1$. The band structure resides in the lower (upper) half of the complex plane when $\rho > 0$ ($\rho < 0$), indicative of the plates being lossy (active).

The topological classification of a generic non-Hermitian operator $\hat{\mathcal{H}} \neq \hat{\mathcal{H}}^\dagger$ requires a biorthogonal basis of left ϕ_n^{L} and right ϕ_n^{R} eigenstates, such that $\hat{\mathcal{H}}^\dagger \phi_n^{\mathrm{L}} = E_n^* \phi_n^{\mathrm{L}}$ and $\hat{\mathcal{H}} \phi_n^{\mathrm{R}} = E_n \phi_n^{\mathrm{R}}$, with E_n generally being complex-valued [22]. In the Supplemental Material [40], we extend the standard non-Hermitian topological band theory to nonlocal operators in continuous platforms [45]. The detailed analysis shows that the Chern number of the nth band is $\mathcal{C}_n^+ = s \times (-1)^{n+1} \mathrm{sgn}(\delta)$ with $\delta = 1 - |\rho|$, and $s = +/-$ for positive/negative bands [40]. As previously noted, $\mathcal{C}_n^- = -\mathcal{C}_n^+$ due to reciprocity. Remarkably, the critical values $\rho = \pm 1$ separate distinct topological phases.

Figures 2(a) and 2(b) show that high-order photonic branches ($n = 2, 3, \ldots,$) remain disconnected in the vicinity of $\rho = 1$. Yet, as $\rho \to 1^-$, their imaginary parts descend along the imaginary frequency axis. At the critical resistivity $\rho = 1$, the bands diverge, touch at infinity, and their topological charges switch sign. The evolution of the $n = 1$ branches is distinct: the gap between the positive and negative frequency spectra is initially open [Fig. 2(c)], but it closes as $\rho \to 1^-$. Specifically, when $\rho = 0.943$, the positive and negative $n = 1$ bands intersect at a single point $\omega_n = -2.55\, i\, c/a$ for $k = 1.36/a$ [Fig. 2(d)]. As the resistivity further increases, this degeneracy extends to a line along the imaginary frequency axis [Fig. 2(e)]. The band gap then reopens for $\rho > 0.943^{-1}$. This specific resistivity range, where the gap remains closed, is dictated solely by the planar geometry of the system [40].

The gapped phases of the PPW are linked by an intermediate series of exceptional points (EPs) [46–50]. These EPs emerge when the $n = 1$ bands intersect over the imaginary axis ($\omega_n' = 0$), resulting in the coalescence of the corresponding pseudospinors. Owing to the system cylindrical symmetry, the EPs form a annulus ring. As the resistivity nears its critical value, $\delta \to 0$, the decay rate of the EPs diverges logarithmically $\omega_n'' \sim (c/a) \ln |\delta|^{-1}$. Thus, the topological phase transition is marked by enhanced absorption, a phenomenon that parallels other photonic systems [22,26–33,51–57].

Figure 2(f) presents the detailed topological phase diagram for $\mathcal{C}_n^+$. Intriguingly, at a given resistivity ρ, the Chern numbers of different bands alternate between $+1$ and -1. According to the principle of bulk-edge correspondence, the gap Chern number is correlated with the net number of reflectionless states that propagate at a material interface [1,2,58]. The gap Chern number is determined by the sum of the contributions from all bands below the gap. For instance, for a gapped system with $-1 < \rho < 1$, the gap Chern number for the pseudospin "+" is given by $\mathcal{C}_{\mathrm{gap}}^+ = -1 + 1 - 1 \ldots$. This sequence is notably nonconvergent, a feature that is quite unique in the realm of topological physics. This property can be attributed to the particle-hole symmetry characteristic of photonic systems [40,59]. Indeed, this symmetry implies that the band diagram comprises an infinite number of bands below the zero-frequency gap, resulting in the nonconvergent series. It is important to contrast this with condensed matter systems, where the total topological charge is always finite due to the existence of a well-defined ground state.

To elucidate the implications of the non-convergent series, we next turn our attention to the edge states at the system boundary and their association with the topological charge. For simplicity, our analysis is concentrated on the $\rho = 0$ case. This is because non-Hermiticity is known to impact [22,28,29,46,60], and in some cases even challenge [61–64], the bulk-edge correspondence. Remarkably, under the Hermitian condition, the label "n" that identifies the bulk bands continues to be a valid quantum number [40]. This remains true even when the waveguide is closed with a $\mathcal{PTD}$-symmetric lateral vertical wall with an arbitrary contour. Thus, the physical waveguide can be conceptualized as a juxtaposition of infinitely many uncoupled virtual waveguides, as sketched in Fig. 3. All the virtual waveguides share a common band gap that separates the positive and negative frequency bands. Each bulk virtual guide describes a degenerate two-band Kane-Mele type model [16].

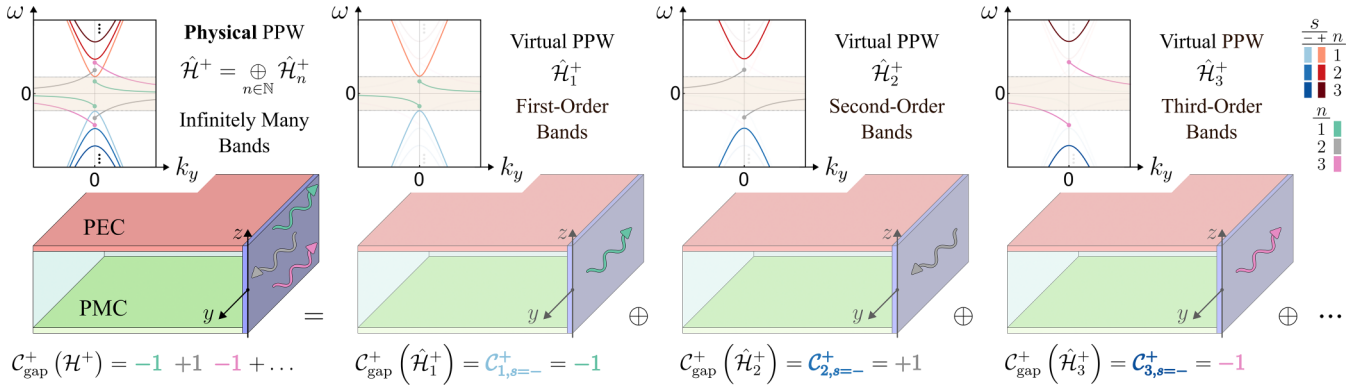

FIG. 3. Conceptualization of the physical guide terminated with the lateral wall as a juxtaposition of infinite virtual guides. For the pseudospin "+", the Hamiltonian $\hat{\mathcal{H}}^+$ is the infinite direct sum of partial Hamiltonians $\hat{\mathcal{H}}_n^+$. Positive/negative bulk modes are shown in red/blue tones. The edge waves associated with the quantum numbers $n = 1, 2, 3$ are marked in green, gray, and pink, respectively. The edge modes are shown pictorially with arrows along the lateral wall and are gapless. The details of the simulations and analytical derivations can be found in the SM [40].

Focusing our attention in the "+" spin polarized waves, the previous discussion shows that the operator $\hat{\mathcal{H}}^+$ can be written as a direct sum of the Hamiltonians associated with the virtual guides: $\hat{\mathcal{H}}^+ = \hat{\mathcal{H}}_1^+ \oplus \hat{\mathcal{H}}_2^+ \oplus \cdots$ (see Fig. 3). The operator $\hat{\mathcal{H}}_n^+$ has a single band below the gap, and has a well-defined topology determined by the "charge" $\mathcal{C}_n^+ = (-1)^n$. Thus, the bulk-edge correspondence implies that each virtual guide supports exactly one "+" polarized unidirectional edge state. The direction of propagation of the edge state of $\hat{\mathcal{H}}_n^+$ is strictly locked to the sign of the respective gap Chern number [58]. In the Supplementary Material, we present closed analytical formulas for the edge states supported by a straight lateral wall [40]. Consistent with the bulk-edge correspondence, each virtual guide accommodates a single gapless edge state (with "+" polarization), with the direction of propagation dependent on the parity of n (see Fig. 3) [40]. Therefore, the physical guide hosts an infinite number of gapless scattering-immune edge-states, each corresponding to a term in the ill-defined series $\mathcal{C}_{\text{gap}}^+ = -1 + 1 - 1 + \ldots$. In this example, the edge-states are backward waves [40].

In summary, we introduced a novel class of non-Hermitian, $\mathcal{PD}$-symmetric, and reciprocal photonic insulators. Our findings demonstrate that, despite the non-Hermitian nature of these systems, Maxwell's equations can be decoupled into spin-up and spin-down states, interconnected by $\mathcal{PD}$-symmetry. Notably, the Chern numbers associated with one of these spin sectors are nonzero, revealing a nontrivial topological characteristic within the sector. We identified two distinct topological phases, differentiated by the degree of material dissipation. The transition between these phases is characterized by the merging of the positive and negative frequency spectra, leading to the formation of a ring of EPs. This phenomenon is particularly significant as it is associated with resonant energy absorption when the impedance of the plates matches that of the dielectric. Moreover, our study uncovered a unique topological phase characterized by a nonconvergent gap Chern number. We elucidated that this peculiar behavior stems from the particle-hole symmetry. By correlating each term of the divergent series with a topologically protected edge state at the system boundary, we have provided a precise interpretation to this otherwise ill-defined series.

This work is partially supported by the IET under the A F Harvey Engineering Research Prize, by the Simons Foundation under the Award No. 733700 (Simons Collaboration in Mathematics and Physics, "Harnessing Universal Symmetry Concepts for Extreme Wave Phenomena"), by Fundação para a Ciência e a Tecnologia and Instituto de Telecomunicações under Project No. UIDB/50008/2020 and by FCT-Portugal through Grant No. 2022.07471.CEECIND/CP1718/CT0001 and in the framework of the Strategic Funding UIDB/04650/2020.

[1] L. Lu, J. D. Joannopoulos, and M. Soljačić, Nat. Photon. **8**, 821 (2014).
[2] M. Kim, Z. Jacob, and J. Rho, Light Sci. Appl. **9**, 130 (2020).
[3] F. D. M. Haldane and S. Raghu, Phys. Rev. Lett. **100**, 013904 (2008).
[4] S. Raghu and F. D. M. Haldane, Phys. Rev. A **78**, 033834 (2008).
[5] F. Liu and J. Li, Phys. Rev. Lett. **114**, 103902 (2015).
[6] K. Y. Bliokh, D. Smirnova, and F. Nori, Science **348**, 1448 (2015).
[7] M. C. Rechtsman, J. M. Zeuner, Y. Plotnik, Y. Lumer, D. Podolsky, F. Dreisow, S. Nolte, M. Segev, and A. Szameit, Nature (London) **496**, 196 (2013).
[8] W. Gao, M. Lawrence, B. Yang, F. Liu, F. Fang, B. Béri, J. Li, and S. Zhang, Phys. Rev. Lett. **114**, 037402 (2015).
[9] A. B. Khanikaev, S. H. Mousavi, W.-K. Tse, M. Kargarian, A. H. MacDonald, and G. Shvets, Nat. Mater. **12**, 233 (2013).
[10] T. Ma, A. B. Khanikaev, S. H. Mousavi, and G. Shvets, Phys. Rev. Lett. **114**, 127401 (2015).

[11] W.-J. Chen, S.-J. Jiang, X.-D. Chen, B. Zhu, L. Zhou, J.-W. Dong, and C. T. Chan, Nat. Commun. **5**, 5782 (2014).
[12] A. Slobozhanyuk, S. H. Mousavi, X. Ni, D. Smirnova, Y. S. Kivshar, and A. B. Khanikaev, Nat. Photon. **11**, 130 (2017).
[13] X. Cheng, C. Jouvaud, X. Ni, S. H. Mousavi, A. Z. Genack, and A. B. Khanikaev, Nat. Mater. **15**, 542 (2016).
[14] C. He, X.-C. Sun, X.-P. Liu, M.-H. Lu, Y. Chen, L. Feng, and Y.-F. Chen, Proc. Natl. Acad. Sci. **113**, 4924 (2016).
[15] M. G. Silveirinha, Phys. Rev. B **93**, 075110 (2016).
[16] C. L. Kane and E. J. Mele, Phys. Rev. Lett. **95**, 146802 (2005).
[17] C. L. Kane and E. J. Mele, Phys. Rev. Lett. **95**, 226801 (2005).
[18] M. G. Silveirinha, Phys. Rev. B **95**, 035153 (2017).
[19] W.-J. Chen, Z.-Q. Zhang, J.-W. Dong, and C. T. Chan, Nat. Commun. **6**, 8183 (2015).
[20] S. Lannebère and M. G. Silveirinha, Nanophotonics **8**, 1387 (2019).
[21] M. G. Silveirinha, Phys. Rev. B **99**, 125155 (2019).
[22] H. Shen, B. Zhen, and L. Fu, Phys. Rev. Lett. **120**, 146402 (2018).
[23] B. Midya, H. Zhao, and L. Feng, Nat. Commun. **9**, 2674 (2018).
[24] C. Poli, M. Bellec, U. Kuhl, F. Mortessagne, and H. Schomerus, Nat. Commun. **6**, 6710 (2015).
[25] M. Pan, H. Zhao, P. Miao, S. Longhi, and L. Feng, Nat. Commun. **9**, 1308 (2018).
[26] C. Dembowski, H.-D. Gräf, H. L. Harney, A. Heine, W. D. Heiss, H. Rehfeld, and A. Richter, Phys. Rev. Lett. **86**, 787 (2001).
[27] H. Xu, D. Mason, L. Jiang, and J. G. E. Harris, Nature (London) **537**, 80 (2016).
[28] D. Leykam, K. Y. Bliokh, C. Huang, Y. D. Chong, and F. Nori, Phys. Rev. Lett. **118**, 040401 (2017).
[29] K. Esaki, M. Sato, K. Hasebe, and M. Kohmoto, Phys. Rev. B **84**, 205128 (2011).
[30] S.-D. Liang and G.-Y. Huang, Phys. Rev. A **87**, 012118 (2013).
[31] T. E. Lee, Phys. Rev. Lett. **116**, 133903 (2016).
[32] H. Menke and M. M. Hirschmann, Phys. Rev. B **95**, 174506 (2017).
[33] H. Zhou, C. Peng, Y. Yoon, C. W. Hsu, K. A. Nelson, L. Fu, J. D. Joannopoulos, M. Soljačić, and B. Zhen, Science **359**, 1009 (2018).
[34] D. E. Fernandes and M. G. Silveirinha, Phys. Rev. Appl. **12**, 014021 (2019).
[35] D. J. Bisharat and D. F. Sievenpiper, Phys. Rev. Lett. **119**, 106802 (2017).
[36] D. J. Bisharat and D. F. Sievenpiper, Laser Photon. Rev. **13**, 1900126 (2019).
[37] X. Cui, R.-Y. Zhang, Z.-Q. Zhang, and C. T. Chan, Phys. Rev. Lett. **129**, 043902 (2022).
[38] R. Roy, Phys. Rev. B **79**, 195321 (2009).
[39] E. Martini, M. G. Silveirinha, and S. Maci, IEEE Trans. Antennas Propagat. **67**, 1035 (2019).
[40] See Supplemental Material at http://link.aps.org/supplemental/10.1103/PhysRevB.109.L241406 for (i) pseudospin-polarization in $\mathcal{PD}$-symmetric reciprocal media; (ii) boundary conditions for the PPW; (iii) bulk modes; (IV) spin Chern numbers; (v) particle-hole symmetry in photonics; (vi) useful limits; (vii) band structure near the phase transition; and (viii) edge states of the PEC-PMC guide terminated by an opaque wall. It also contains Refs. [41–43].
[41] J. A. Nelder and R. Mead, Comput. J. **7**, 308 (1965).
[42] P.-S. Kildal, Electron. Lett. **24**, 168 (1988).
[43] P.-S. Kildal, IEEE Trans. Antennas Propag. **38**, 1537 (1990).
[44] D. N. Sheng, Z. Y. Weng, L. Sheng, and F. D. M. Haldane, Phys. Rev. Lett. **97**, 036808 (2006).
[45] M. G. Silveirinha, Phys. Rev. B **92**, 125153 (2015).
[46] M.-A. Miri and A. Alù, Science **363**, eaar7709 (2019).
[47] M. Berry, Czech. J. Phys. **54**, 1039 (2004).
[48] M. V. Keldysh, Russ. Math. Surv. **26**, 15 (1971).
[49] T. Kato, *Perturbation Theory for Linear Operators* (Springer Science & Business Media, New York, 2013), Vol. 132.
[50] N. Moiseyev, *Non-Hermitian Quantum Mechanics* (Cambridge University Press, Cambridge, England, 2011).
[51] R. Uzdin, A. Mailybaev, and N. Moiseyev, J. Phys. A: Math. Theor. **44**, 435302 (2011).
[52] M. Berry and R. Uzdin, J. Phys. A: Math. Theor. **44**, 435303 (2011).
[53] M. V. Berry, J. Opt. **13**, 115701 (2011).
[54] I. Gilary, A. A. Mailybaev, and N. Moiseyev, Phys. Rev. A **88**, 010102(R) (2013).
[55] E.-M. Graefe, A. A. Mailybaev, and N. Moiseyev, Phys. Rev. A **88**, 033842 (2013).
[56] T. J. Milburn, J. Doppler, C. A. Holmes, S. Portolan, S. Rotter, and P. Rabl, Phys. Rev. A **92**, 052124 (2015).
[57] J. Doppler, A. A. Mailybaev, J. Böhm, U. Kuhl, A. Girschik, F. Libisch, T. J. Milburn, P. Rabl, N. Moiseyev, and S. Rotter, Nature (London) **537**, 76 (2016).
[58] M. G. Silveirinha, Phys. Rev. X **9**, 011037 (2019).
[59] F. R. Prudêncio and M. G. Silveirinha, Phys. Rev. Lett. **129**, 133903 (2022).
[60] F. K. Kunst, E. Edvardsson, J. C. Budich, and E. J. Bergholtz, Phys. Rev. Lett. **121**, 026808 (2018).
[61] S. Yao and Z. Wang, Phys. Rev. Lett. **121**, 086803 (2018).
[62] F. K. Kunst and V. Dwivedi, Phys. Rev. B **99**, 245116 (2019).
[63] C. H. Lee and R. Thomale, Phys. Rev. B **99**, 201103(R) (2019).
[64] S. Longhi, Opt. Lett. **46**, 6107 (2021).